*ENGINEERING TRANSACTIONS* • *Engng. Trans.* • **43**, 1–2, 45–70, 1995
Polish Academy of Sciences • Institute of Fundamental Technological Research

# AN INTERACTIVE PROGRAM FOR SHAPE OPTIMIZATION OF SECTIONS UNDER SAINT–VENANT TORSION USING BOUNDARY ELEMENT METHOD (*)

P. BERKOWSKI, J.M. SIECZKOWSKI (WROCŁAW)

and M. DOBLARÉ, L. GRACIA (ZARAGOZA)

An interactive program for visualization of results generated during the shape optimization of simply and multiply-connected isotropic sections under the Saint-Venant torsion using B.E.M. is presented in this paper. The program includes some graphical tools essential for preprocessing, analysis and postprocessing parts of the optimization system and makes it possible to carry out boundary mesh modifications caused by changes in its geometry and initial mesh, and also by the intersecting boundaries. In order to show the influence of the geometric irregularities and intersections of the boundaries on the optimization process as well as the advantages of the program proposed, some examples of the shape optimization are presented.

## 1. INTRODUCTION

Shape optimization of elastic solids under various loads is a very common problem in civil engineering and mechanical system design. A lot of reasons have caused the increasing interest and progress in this field: general evolution of such methods as F.E.M. and B.E.M., the development of new numerical linear and nonlinear optimization algorithms with multiple constraints, and introduction of new, powerful computers.

As mentioned above, both the methods of analysis (F.E.M. and B.E.M.) are used in solving general shape optimization problems, the basis of which has been broadly presented by SOKOŁOWSKI and ZOLESIO in [1] and, in particular, in shape optimization of shafts subject to torsion (DEMS [2], KIKUCHI [3], KURSHIN [4]), what also is the subject of this paper. However, application of finite elements in shape optimization presents some disadvantages, such as the necessity of meshing of the entire domain and very

(*) Paper presented at 30th Polish Solid Mechanics Conference, Zakopane, September 5–9, 1994.

laborious and difficult mesh redefinition. The same was observed by HOU and SHEEN [5] who compared the optimization and sensivity design schemes based on both methods.

Application of the B.E.M. as an approximation method in shape optimization allows us to avoid these disadvantages. MOTA *et al.* [6, 7] have developed some particular models for the optimum shape design of hollow shafts based on maximization of the torsional stiffness. A similar model has been proposed by BURCZYŃSKI and ADAMCZYK [8, 9] by formulating the optimality condition and using the Newton–Raphson method to solve the nonlinear problem. A very extensive discussion on different approaches to this problem is presented by GRACIA *et al.* in [10, 11, 12, 13] containing a general description of the shape optimization model for 2D elastic bodies, including hollow shaft shape optimization. KOBELEV described in [14] an optimization problem aimed at finding the optimal shape for an elastic bar in torsion with minimization of the stress concentration. Recently ZHAO and ADEY [15, 16] presented main elements of shape optimization with the material derivative and design sensivity analysis.

The second aspect of the shape optimization problem under consideration, besides the method of analysis, is the computational one, concerning the way of incorporating computer analysis programs into the global optimal shape design procedure.

ATREK [17] has designed a program to be used in production environment. The program is integrated with the finite element analysis program and compatible with that for pre- and postprocessing. A general concept of an optimization system has been developed by KIBSGAARD *et al* [18]. In that system they define the optimization problem within a general CAD-system for pre- and postprocessing and for any finite element analysis program. An interactive system for structural design sensivity and optimization, based on the F.E.M., has been introduced by SANTOS *et al.* [19]. A menu-driven system in a multi-window graphics-based workstation is used to assist the interactive performance. ARIAS *et al.* [20] developed a structural model for a geometric representation oriented towards an automatic shape optimal design, based on a CAD model and the finite element analysis model.

A very brief presentation of the shape optimization background, included in this paper, obviously does not cover all the aspects and advances achieved in this field in the last decades. However, its aim is to point out some of the most important problems that caused the interest in developing a graphical tool which could facilitate the solution of some problems that appear during the shape optimum design.

An interactive program for visualization the results generated during the shape optimization of simply and multiply-connected isotropic sections under Saint-Venant torsion by using B.E.M. is presented and discussed in this paper [21]. The program incorporates some graphical tools essential for preprocessing, analysis and postprocessing parts of the optimization system and allows us to carry out the boundary mesh modifications caused by changes in its geometry and initial mesh, and by the boundary intersections. At the present stage, the optimization program includes only the shape optimization problem defined for simply and multiply-connected isotropic sections subjected to the Saint-Venant torsion. The optimization problem is formulated so as to obtain the given torsional stiffness under the minimum area condition, and the expression of the stiffness is established as a function of boundary integrals which depend on state variables based on the nodes coordinates of the boundary. The variables are obtained by means of the B.E.M. To solve the optimization problem, a method based on the ideas of the feasible direction methods and the gradient methods are employed.

## 2. Basic elements of an interactive graphical program

The proposed interactive program for definition, visualization and modification of the shape optimization problem and results consists of two fundamental parts: the graphical unit used to define and redefine the problem geometry (graphical pre- and postprocessors), and the optimization unit that performs the design process, basing its analytic part on the B.E.M. A general idea of an interactive work with the program consists in giving to a program user a possibility to define graphically the geometry of an initial shape to be optimized, and then to have a chance to observe the optimization process at any iteration step. The program gives information about the current design by its graphical presentation on the screen, allows us to introduce all necessary changes in the boundary mesh, and then enables us to continue the design process until the optimal shape is obtained.

The graphical unit of the DIFOPTI program contains a group of geometrical tools (calculation of boundary element length, areas contained within the boundaries and angles between the elements, detection of boundary intersections and mesh redefinition), completed by those of the visual presentation of optimized shapes (drawing of boundaries with different zoom levels, graphical presentation of the objective function and restriction evolution).

The process of data preparation for the shape optimization problem by means of the DIFOPTI interactive program, that can be performed in a numerical or a graphical mode, consists of the three following parts:

- definition of general parameters that direct the optimization method;
- introduction of additional information to carry out the mesh redefinition;
- definition of initial shape geometry.

After hierarchy organized general menu offers to the user the capabilities for making definition of the design problem by using tree defined sub-menus (Figs. 1, 2). Selections can be made through the use of a mouse. The mouse button is used to realize selections from different button-menus and from the keyboard printed on the screen. The data can be introduced in a numerical manner from the keyboard, or by "drawing" it on the screen.

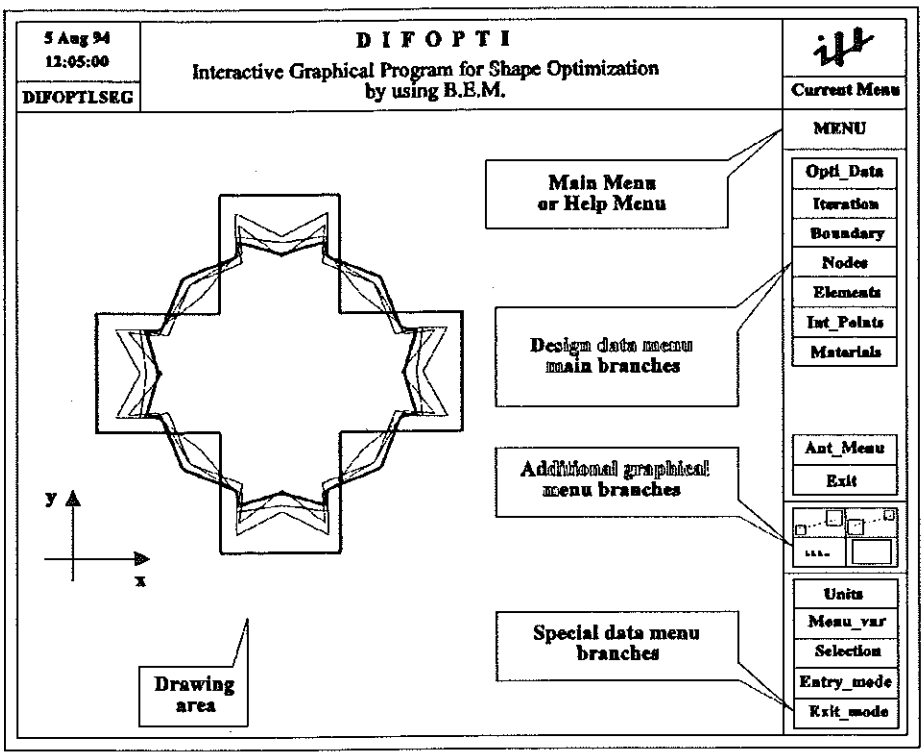


FIG. 1. Main menu system.

The user begins a definition of any shape optimization problem with defining some general parameters that are included in the Opti_Data menu:

- General problem data that have to be defined numerically (number of the example, maximum number of iterations, maximum value of an angle between elements; parameter of geometrical redefiniton type and checking element's length, bound adjusting parameter, stiffness constraint, constraint error value, error value at the minimum).

• General problem data which can be defined numerically or graphically in defining the initial shape (number of origins, boundaries, nodes, elements, internal points and materials).

In other menus (Fig. 1) of the main branch menu, the user defines the initial shape of a section to be optimized. Every one of them contains some graphical sub-menus, such as: definition, modification, cutting, listing and drawing of its elements (Fig. 2).

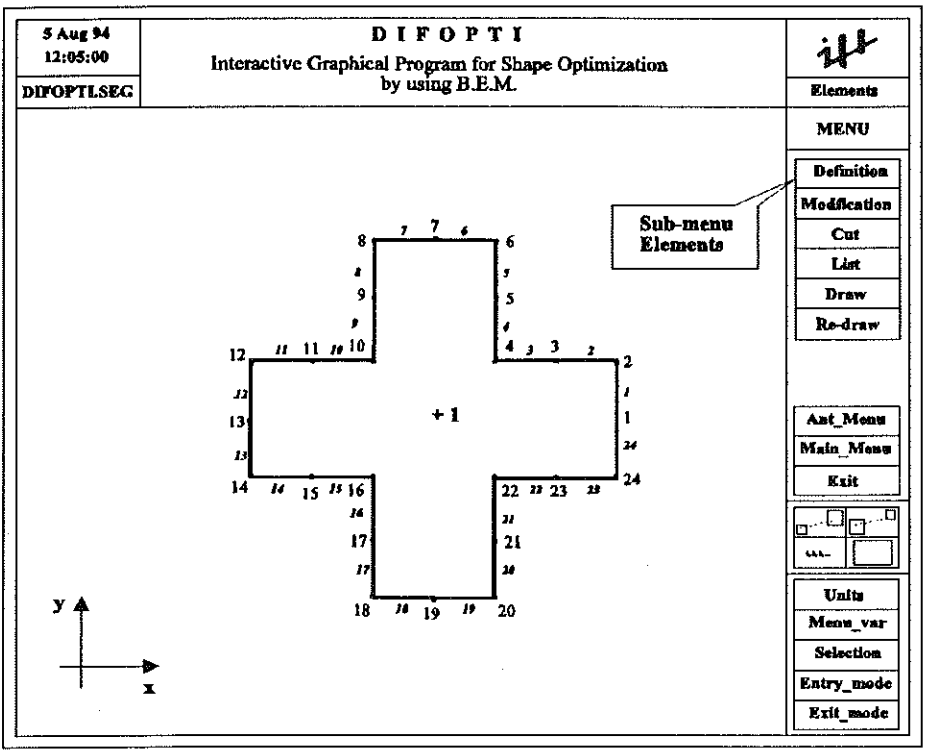


FIG. 2. Sub-menu system.

The user has also the possibility of editing the shape on the screen by its enlargement, reduction and clearing. These options are included in additional graphical menu. A special data menu contains some options which allows to define the units, select the groups of any variables to be edited, and to define the type of data entry (graphical or numerical) and data exit (file, screen, etc.).

At the present stage, the DIFOPTI graphical program has been connected to the shape optimization program of sections under the Saint-Venant torsion based on the formulation presented in [10, 11, 12].

## 3. Mesh redefinition during optimization process

### *3.1. Introduction*

The optimization process leads to redefinition of the initial boundary geometry until it gets the optimal shape. However, this process can produce irregularities in the boundary geometry or the boundary mesh at any iteration step. In this case it is necessary to include in the program different safeguards, in order to guarantee the convergence of the process and the fulfilment of geometric restrictions.

In general, there are three main types of the irregularities which necessitate the mesh redefinition and which should be detected during the optimization process. They are [10, 11, 12, 21]:

- geometric irregularities;
- variation in mesh element's length;
- intersectiones of boundaries.

### *3.2. Geometrical mesh irregularities*

The evolution of the shape design during the optimization process can result in the appearance of acute angles between the mesh elements, which may slow down the convergence of the iterative process. In order to avoid the problem of acute corners, they are detected by calculating the scalar product of the normals of two adjoning elements (Fig. 3a):

$$\cos\alpha = -\mathbf{n}_{j-1} \cdot \mathbf{n}_j \leq \cos\alpha_0. \tag{3.1}$$

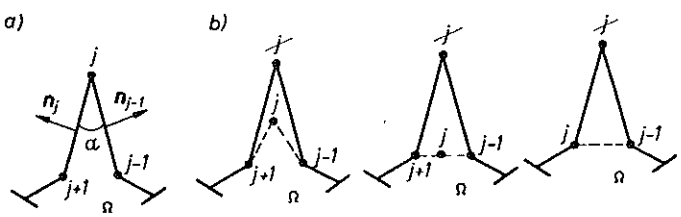


FIG. 3. Geometrical mesh irregularities and redefinition; a) initial mesh with acute angle, b) mesh redefinition.

If the value of $\cos\alpha \geq \cos\alpha_0$ ($\alpha_0$ – an arbitrary limit angle), the mesh is to be redefined by changing the coordinates of the node introducing acute angle between elements. New coordinates can be calculated depending on

the geometrical situation (Fig. 3) using one of the two following equations:

$$\mathbf{x}'_j = \frac{\mathbf{x}_{j-1} + \mathbf{x}_{j+1}}{2}, \tag{3.2}$$

$$\mathbf{x}'_j = \frac{1}{2}\left(\mathbf{x}_j + \frac{\mathbf{x}_{j-1} + \mathbf{x}_{j+1}}{2}\right), \tag{3.3}$$

where $\mathbf{x}$, $\mathbf{x}'$ are vectors of the old and new coordinates, respectively, or by removing the node with acute angle and its adjacent elements and defining a new element between the previous node and the next one (Fig. 3b). A relatively fine mesh is necessary to complete this action, and also an analysis of the lengths of the elements is necessary at each optimization step.

### *3.3. Length distorsion of mesh elements*

As a consequence of the changes of nodal coordinates during the optimization process or as a consequence of the changes caused by elimination of the mesh irregularities, important variations of element length can appear. To solve this problem, a study of the lengths of the elements must be carried out at each iteration step, redefining the mesh when it proves to be necessary.

In case of the element length greater $a$ times than the mean value $L_m$ ($a = 1.5$ in this study), the element is divided by introducing some new nodes ($n$) along the element (Fig. 4a) according to the following criterion:

$$n = a \cdot (L/L_m). \tag{3.4}$$

In case when the length is less than $L_m/a$, the element should be removed (Fig. 4b).

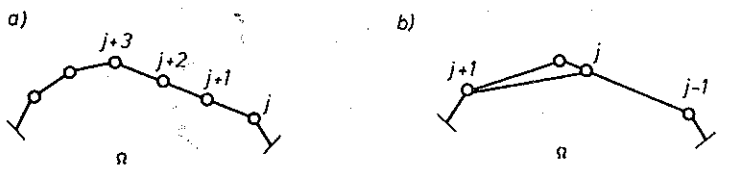


FIG. 4. Checking of element's length; a) long elements, b) short elements.

The mean length value ($L_m$) is calculated for each boundary as the mean value of the lengths of its elements, or as the mean length of all the elements belonging to all the boundaries that compose the optimized shape.

### *3.4. Intersection of boundaries*

If we optimize a multiply-connected domain, it is possible to obtain the intersections between its boundaries. This enables us to avoid the erroneous results.

The procedure of detecting the boundary intersections is based on determination of the value of the integral

$$\mathbf{I} = \int_{\Gamma} \frac{\mathbf{r} \cdot \mathbf{n}}{r^2} d\Gamma. \tag{3.5}$$

Values of integral **I** (3.6) depend upon the position of the reference point $P$ (origin of radius **r**) with respect to the boundary over which we integrate. Two different cases should be taken into account (Fig. 5):

- Intersection of a boundary with itself (it can happen to an internal or an external boundary).
- Intersection of two boundaries (two internal boundaries or an external and an internal one).

$$\begin{aligned} &\mathbf{I} = 2\pi \quad \text{if} \quad P \in \Omega, \\ &\mathbf{I} = \pi \quad \text{if} \quad P \in \Gamma, \\ &\mathbf{I} = 0 \quad \text{if} \quad P \notin \Omega + \Gamma. \end{aligned} \tag{3.6}$$

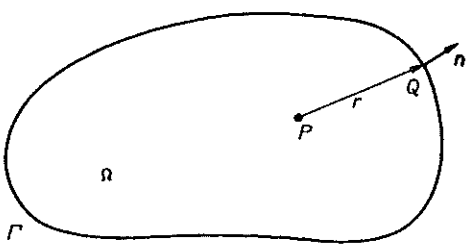


FIG. 5. Values of integral **I**.

#### *a. Intersection of external or internal boundary with itself*

In that case we look for a change of the sign of the integral **I**, when it is computed in all the nodes which belong to this boundary (Fig. 6). Its values are as follows:

$$\begin{aligned} \mathbf{I}_P &= \int_{\Gamma_1} + \int_{\Gamma_2} = \pi + 0 = \pi, \\ \mathbf{I}_Q &= \int_{\Gamma_1} + \int_{\Gamma_2} = 0 + (-\pi) = -\pi. \end{aligned} \tag{3.7}$$

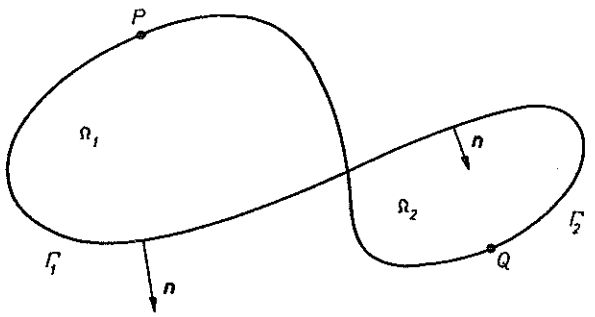


FIG. 6. Intersection of a boundary with itself.

*b. Intersection of two boundaries*

*Intersection of internal and external boundaries.* In this case we determine the value of the integral **I** computed in the nodes of the internal boundary $\Gamma_1$ with respect to the external one, $\Gamma_2$ (Fig. 7). Its values are as follows:

$$\mathbf{I}_P = \int_\Gamma = 2\pi \quad \text{if} \quad P \in \Omega_0,$$

$$\mathbf{I}_P = \int_\Gamma = \pi \quad \text{if} \quad P \in \Gamma_0, \tag{3.8}$$

$$\mathbf{I}_P = \int_\Gamma = 0 \quad \text{if} \quad P \notin \Omega_0 + \Gamma_0.$$

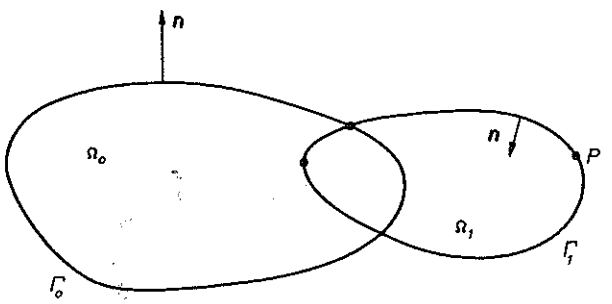


FIG. 7. Intersection of internal and external boundaries.

*Intersection of two internal boundaries.* In this case we also determine the value of the integral **I** computed in the nodes of the internal boundary

$\Gamma_1$ with respect to the external one, $\Gamma_2$ (Fig. 8). Its values are as follows:

$$\mathbf{I}_P = \int_{\Gamma_2} = 0 \quad \text{if} \quad P \notin \Omega_2 + \Gamma_2,$$

$$\mathbf{I}_P = \int_{\Gamma_2} = -\pi \quad \text{if} \quad P \in \Gamma_2, \tag{3.9}$$

$$\mathbf{I}_P = \int_{\Gamma_2} = -2\pi \quad \text{if} \quad P \in \Omega_2.$$

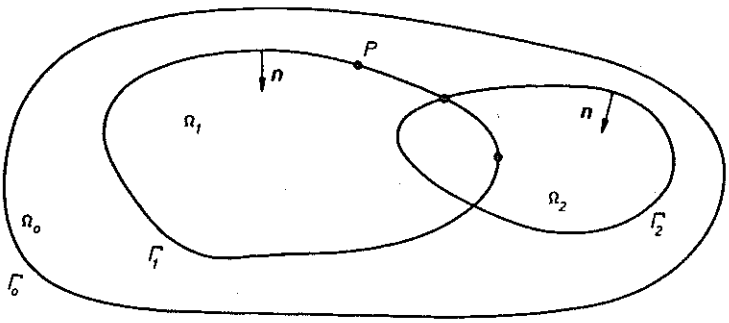


FIG. 8. Intersection of two internal boundaries.

All the cases of boundary irregularities are detected automatically during the optimization process and are eliminated after breaking the iteration process, an interactive graphical boundary mesh redefinition being used.

## 4. Formulation of Saint–Venant torsion problem by using B.E.M.

### *4.1. Formulation of torsion problem for isotropic solids*

The solution of the Saint-Venant torsion problem described in this chapter is based on that formulated by GRACIA [10] and GRACIA and DOBLARÉ in [11, 12], where they presented a general problem of shape optimization of 2D elastic bodies based on the boundary element method. To formulate the Saint-Venant torsion problem for isotropic and homogenous solids and for multiply-connected domains (Fig. 9), we can use the so-called Prandtl function, obtaining a Poisson equation:

$$\frac{\partial^2 \phi}{\partial x^2} + \frac{\partial^2 \phi}{\partial y^2} = -2 \quad \text{in} \quad \Omega, \tag{4.1}$$

with

$$\phi_i = k_i \qquad \text{in} \quad \Gamma_i, \quad i = 0, 1, \ldots, N, \tag{4.2}$$

where $N$ is the number of boundaries,

$$\int_{\Gamma_i} \frac{\partial \phi}{\partial \mathbf{n}} d\Gamma_i = -2A_i, \qquad i = 1, \ldots, N, \tag{4.3}$$

and where

$$A_i = \frac{1}{2} \sum_{j=1}^{N^i} (\mathbf{r}_j \cdot \mathbf{n}_j) L_j \tag{4.4}$$

is the area enclosed by each internal boundary, $N^i$ is the number of elements of each internal boundary, $L_j$ is the length of the $j$-th element, $\mathbf{n}_j$ is the normal to it, and $\mathbf{r}_j$ is the radius-vector between the element and the origin of coordinates.

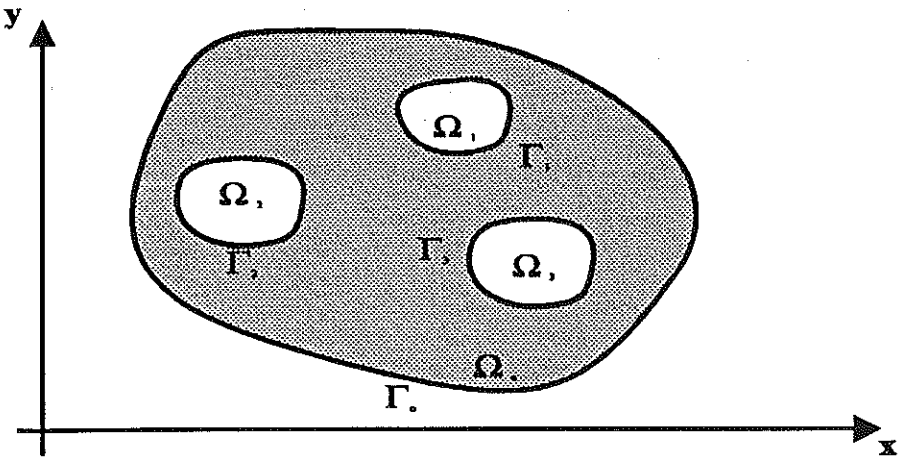


FIG. 9. Two-dimensional multiply-connected domain.

The tangential stresses at any point can be written in the following form:

$$\begin{aligned} \tau_{xz} &= G\Theta \frac{\partial \phi}{\partial y}, \\ \tau_{yz} &= -G\Theta \frac{\partial \phi}{\partial x}, \end{aligned} \tag{4.5}$$

where $G$ is the shear modulus and $\Theta$ is the twist per unit length.

The magnitude of the tangential stress is expressed by

$$\tau = G\Theta \sqrt{\left(\frac{\partial \phi}{\partial x}\right)^2 + \left(\frac{\partial \phi}{\partial y}\right)^2} \tag{4.6}$$

and, taking into consideration that the tangential stress has no normal component, we obtain

$$\frac{\partial \phi}{\partial x} = n_x \frac{\partial \phi}{\partial \mathbf{n}}, \qquad \frac{\partial \phi}{\partial y} = n_y \frac{\partial \phi}{\partial \mathbf{n}}, \tag{4.7}$$
$$\tau = G\Theta \left| \frac{\partial \phi}{\partial \mathbf{n}} \right|.$$

The torsional moment can be expressed by

$$M = D\Theta, \tag{4.8}$$

where $D$ is the torsional stiffness defined by (with $N$ denoting the number of boundaries)

$$D = 2G \left[ \int_{\Omega} \phi \, d\Omega - \sum_{i=1}^{N} k_i A_i \right]. \tag{4.9}$$

After solving Eqs. (4.1) – (4.3) we obtain $\phi$, and then the torsional rigidity from Eq. (4.9). If the torsional moment is given, we can calculate the value of $\Theta$ from Eq. (4.8), and then the tangential stresses from Eqs. (4.5) and (4.6).

### *4.2. B.E.M. formulation of Saint – Venant torsion problem*

The introduction of the second Green's identity between the Prandtl function (4.1) and the fundamental solution of the Laplace equation leads to an alternative formulation of Eq. (4.1) in terms of boundary integrals [10, 11, 12]:

$$c(Q)\phi(Q) + \int_{\Gamma} \phi \frac{\partial}{\partial \mathbf{n}} \left( \ln \frac{1}{r} \right) d\Gamma = \int_{\Gamma} \frac{\partial \phi}{\partial \mathbf{n}} \ln \frac{1}{r} - \int_{\Omega} \nabla^2 \phi \ln \frac{1}{r} d\Omega, \tag{4.10}$$

where the constant $c$ takes the values as shown in Fig. 10 and $r$ is the radius-vector joining boundary points and the origin of the coordinate system (Fig. 11).

Value of the constant $c(Q)$ for $Q \in \Gamma$ corresponds to the principal value of the integral

$$\int_{\delta B_\varepsilon(Q)} \frac{\partial}{\partial \mathbf{n}} \left[ \ln \frac{1}{r} \right] d\Gamma, \tag{4.11}$$

where $B_\varepsilon(Q)$ is the unit circle centered at $Q$ and with radius $\varepsilon$, and $\delta B_\varepsilon(Q)$ its boundary. This principal value is equal to the angle subtended by the left and right-hand tangent to $\Gamma$ at $Q$.

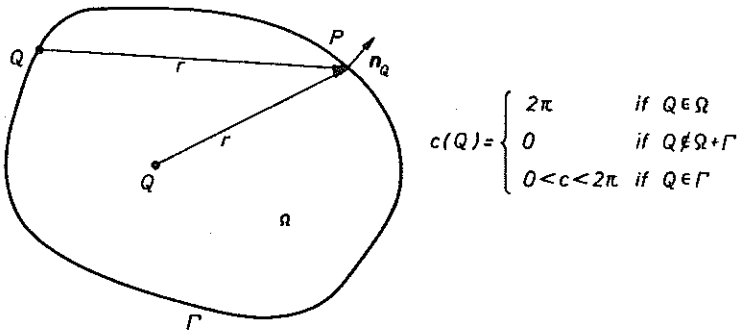


FIG. 10. Values of the constant $c$.

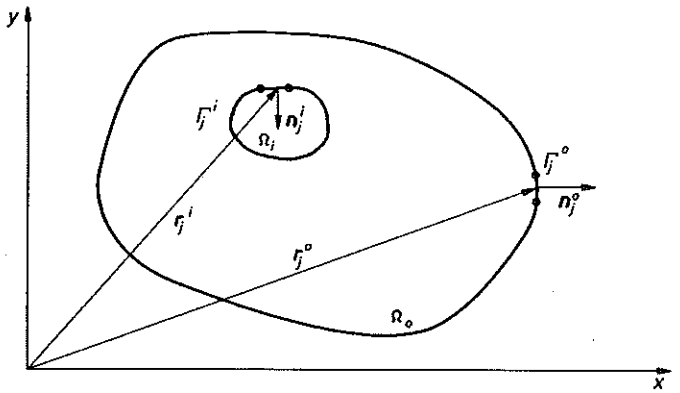


FIG. 11. Definition of the geometry.

To transform the last integral in Eq. (4.10) we can use Eq. (4.1), what allows us to obtain the basic equation of B.E.M.:

$$c(Q)\phi(Q) - \int_\Gamma \phi \frac{\mathbf{r}\cdot\mathbf{n}}{r^2} d\Gamma = -\int_\Gamma \frac{\partial \phi}{\partial \mathbf{n}} \ln r + \int_\Gamma \left(\frac{1}{2} - \ln r\right)(\mathbf{r}\cdot\mathbf{n})\, d\Gamma. \tag{4.12}$$

Using a similar way, we can transform Eq. (4.9) for the torsional stiffness into the boundary integral function:

$$D = -G\left[\frac{1}{4}\int_\Gamma r^2(\mathbf{r}\cdot\mathbf{n})\, d\Gamma + \frac{1}{2}\int_\Gamma \frac{\partial \phi}{\partial \mathbf{n}} r^2\, d\Gamma\right]. \tag{4.13}$$

If we approximate the normal derivative of the Prandtl function $q^i = (\partial\phi/\partial\mathbf{n})^i$ for every boundary (with $\phi^i$ values constant along the boundary) using the following form:

$$q^i = \sum_{j=1}^{N^i} q_j^i \varphi_j, \tag{4.14}$$

where $\varphi_j$ represents the approximation function (in this paper the simplest constant and linear aproximations have been included), $q_j^i$ are new unknown variables, $N^{ei}$ is the number of elements of the boundary $\Gamma_i$ (Fig. 12), Eq. (4.13) can be formulated in the form

$$c(Q)\phi(Q) - \sum_{i=0}^{N} k_i \sum_{j=1}^{N^{ei}} \int_{\Gamma_j} \frac{\mathbf{r}\cdot\mathbf{n}}{r^2} d\Gamma = -\sum_{i=0}^{N}\sum_{j=1}^{N^{ei}}\sum_{k=1}^{2} q_j^k \int_{\Gamma_j} \varphi_k \ln r \, d\Gamma + \sum_{i=0}^{N}\sum_{j=1}^{N^{ei}} \int_{\Gamma_j} \left(\frac{1}{2} - \ln r\right)(\mathbf{r}\cdot\mathbf{n})\, d\Gamma. \tag{4.15}$$

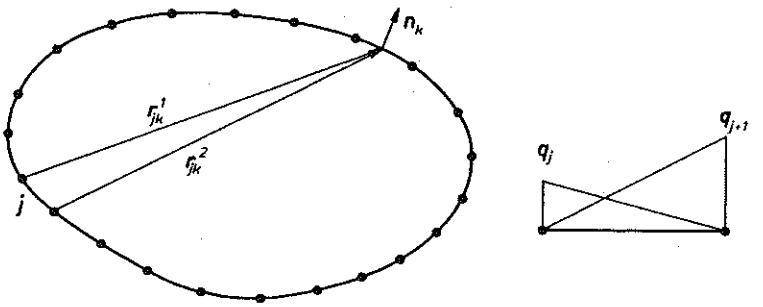


FIG. 12. Boundary nodes and unknowns.

If the Eq. (4.15) is calculated in all nodes of the boundary, we obtain a system of $N^e$ equations with $N^e + \Sigma N^i - 1$ unknowns. These $\Sigma N^i - 1$ additional unknowns correspond to the values of the Prandtl function along the internal boundaries with $\phi$ arbitrarily assumed to be equal zero along the external boundary ($k_0 = 0$). So we obtain the final equation

$$\begin{bmatrix} \mathbf{G} & \mathbf{H} \\ \mathbf{L} & \mathbf{0} \end{bmatrix} \begin{bmatrix} \mathbf{q} \\ \mathbf{k} \end{bmatrix} = \begin{bmatrix} \mathbf{p} \\ \mathbf{a} \end{bmatrix}. \tag{4.16}$$

Using Eq. (4.4) for all the internal boundaries we obtain

$$\frac{1}{2}\sum_{j=1}^{N^i}\sum_{k=1}^{2} q_j^k L_j = -\sum_{j=1}^{N^i}(\mathbf{r}_j \cdot \mathbf{n}_j) L_j \,. \tag{4.17}$$

Elements of the matrices of Eq. (4.16) are defined as stated below:

**H** – matrix that corresponds to the left-hand side part of Eq. (4.15),
**G** – matrix of the first right-hand side integral of Eq. (4.15),
**p** – vector of the second right-hand side integral of Eq. (4.15),
**q**, **k** – represent vectors of unknowns,
**L** – represents a diagonal matrix of lengths of the internal boundaries,
**a** – represents a vector of areas enclosed by internal boundaries.

The torsional stiffness can be then expressed by

$$D = -G\left[\frac{1}{4}\sum_{i=0}^{N}\sum_{j=1}^{N^{ei}}\int_{\Gamma_j} r^2(\mathbf{r}\cdot\mathbf{n})d\Gamma_j + \frac{1}{2}\sum_{i=0}^{N}\sum_{j=1}^{N^{ei}}\sum_{k=1}^{2} q_j^k \int_{\Gamma_j}\varphi_k r^2\, d\Gamma_j\right] \tag{4.18}$$

or in an equivalent form, by

$$D = -G\left[\frac{1}{4}\sum_{i=0}^{N}\sum_{j=1}^{N^{ei}}(I_j^i)_2 + \frac{1}{2}\sum_{i=0}^{N}\sum_{j=1}^{N^{ei}} q_j (I_j^i)_1\right]. \tag{4.19}$$

Integrals in Eqs. (4.15) and (4.18) are calculated, in general, using numerical integration formulae (Gauss quadrature rules). However, in the presence of the singularity due to the fundamental solution, more accurate integration methods, based on special transformations, are used.

## 5. Formulation of optimization problem

The problem of shape optimization of sections subject to the Saint–Venant torsion can now be stated as it was formulated with details in [10, 11, 12, 13]:

Obtain the shape of the section with minimum area having a given torsional stiffness, fulfilling certain constraints related to the section geometry. It should be mentioned that as its dual problem, the problem of finding the section of a given area and maximum torsional stiffness could also be considered.

These additional constraints are as follows:

- some coordinates of the nodes can be bound;
- some boundary nodes can be fixed;
- the boundaries cannot intersect;
- symmetry conditions have to be fulfilled.

The objective function is then defined by

$$f(\mathbf{x}) = \frac{1}{2}\sum_{i=0}^{N}\sum_{j=1}^{N^{ei}}(\mathbf{r}_j\cdot\mathbf{n}_j)L_j \tag{5.1}$$

and the restriction corresponding to the torsional stiffness is

$$h(\mathbf{x}) = 1 - \frac{D}{D_0} = 0 \tag{5.2}$$

or, in an equivalent form,

$$h(\mathbf{x}) = D_0 + G\left[\frac{1}{4}\sum_{i=0}^{N}\sum_{j=1}^{N^{ei}}(I_j^i)_2 + \frac{1}{2}\sum_{i=0}^{N}\sum_{j=1}^{N^{ei}} q_j(I_j^i)_1\right], \tag{5.3}$$

where $D$ is defined by Eq. (4.18), and in this first approximation to the optimization problem, the non-restricted boundary node coordinates have been taken as the design variables $\mathbf{x}$.

The method used in the optimization problem is based on the feasible direction method and the gradient projection method, with some modifications that tend to avoid some disadvantages, as it is described in [10, 11]. It is necessary to add that the restriction imposed on the torsional stiffness can be transformed into "the constraint strip" by using the error bound $\varepsilon_r$, so that the restriction is satisfied when

$$(1 - \varepsilon_r) \leq \frac{D}{D_0} \leq (1 + \varepsilon_r), \tag{5.4}$$

where $D$ is the torsional stiffness of the current design and $D_0$ is the constraint stiffness.

The next important remark concerns the method of automatic constraint strip adjustment at each iteration step, as is presented in Fig. 13.

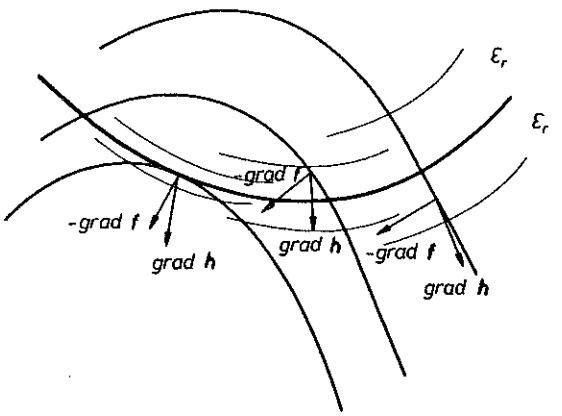


FIG. 13. Constraint strip adjusting.

When the solution approximates the minimum, the angle between $-\text{grad}\,\mathbf{f}$ and $\text{grad}\,\mathbf{h}$ tends to 0 and, in some situations, it is impossible for the incorporated optimization method to reach the minimum, so it is necessary to include some saveguards to avoid this impossibility.

It is completed by defining the error bound $\varepsilon_r'$:

$$\cos\varphi = \frac{\text{grad}\,\mathbf{h}\,\text{grad}\,\mathbf{f}}{|\text{grad}\,\mathbf{h}| \cdot |\text{grad}\,\mathbf{f}|}, \tag{5.5}$$

$$\varphi \leq \varphi_0 = \cos(\pi - \varepsilon_m), \tag{5.6}$$

$$\varepsilon_r' = (\sin(\arcsin(\varphi))^2 < \varepsilon_r\,, \tag{5.7}$$

where $\varepsilon_m$ is the admissible error in the minimum for the Kuhn–Tucker condition (an angle between $-\text{grad}\,\mathbf{f}$ and $\text{grad}\,\mathbf{h}$).

Each iteration step requires the calculation of the objective function (5.1) gradient and the constraint (5.2) gradient with respect to the coordinates (design variables). The objective function gradient with respect to the node coordinates is calculated directly (5.8), while the constraint gradient (5.9) needs derivation of the Prandtl function and its normal derivatives. These derivatives are obtained as follows:

$$\begin{aligned} \frac{\partial f(\mathbf{x})}{\partial x_i} &= \frac{y_{i+1} - y_{i-1}}{2}\,, \\ \frac{\partial f(\mathbf{x})}{\partial y_i} &= \frac{x_{i-1} - x_{i+1}}{2}\,, \end{aligned} \tag{5.8}$$

where $(i-1)$ and $(i+1)$ are the anterior and the posterior nodes, respectively, and

$$\frac{\partial h(\mathbf{x})}{\partial x_i} = \frac{1}{4}\frac{\partial}{\partial x_i}[(I_i)_2 + (I_{i-1})_2] + \frac{1}{2}\sum_{i=0}^{N}\sum_{j=1}^{N^{ei}}\left[\frac{\partial q_j}{\partial x_i} I_1^j + q_j \frac{\partial I_1^i}{\partial x_i}\right]. \tag{5.9}$$

To obtain the value of the derivatives of state variables $q_j$, it is necessary to calculate at each iteration step the direct derivative of the equation system (4.16) in the form of

$$\begin{bmatrix} \dfrac{\partial \mathbf{G}}{\partial x_i} & \dfrac{\partial \mathbf{H}}{\partial x_i} \\ \dfrac{\partial \mathbf{L}}{\partial x_i} & \mathbf{0} \end{bmatrix} \begin{bmatrix} \mathbf{q} \\ \mathbf{k} \end{bmatrix} + \begin{bmatrix} \mathbf{G} & \mathbf{H} \\ \mathbf{L} & \mathbf{0} \end{bmatrix} \begin{bmatrix} \dfrac{\partial \mathbf{q}}{\partial x_i} \\ \dfrac{\partial \mathbf{k}}{\partial x_i} \end{bmatrix} = \begin{bmatrix} \dfrac{\partial \mathbf{p}}{\partial x_i} \\ \dfrac{\partial \mathbf{a}}{\partial x_i} \end{bmatrix} \tag{5.10}$$

and in order to separate $\partial\mathbf{q}/\partial\mathbf{x}$ and $\partial\mathbf{k}/\partial\mathbf{x}$,

$$\begin{bmatrix} \dfrac{\partial \mathbf{q}}{\partial x_i} \\ \dfrac{\partial \mathbf{k}}{\partial x_i} \end{bmatrix} = \begin{bmatrix} \mathbf{G} & \mathbf{H} \\ \mathbf{L} & \mathbf{0} \end{bmatrix}^{-1} \left[ \begin{bmatrix} \dfrac{\partial \mathbf{p}}{\partial x_i} \\ \dfrac{\partial \mathbf{a}}{\partial x_i} \end{bmatrix} - \begin{bmatrix} \dfrac{\partial \mathbf{G}}{\partial x_i} & \dfrac{\partial \mathbf{H}}{\partial x_i} \\ \dfrac{\partial \mathbf{L}}{\partial x_i} & \mathbf{0} \end{bmatrix} \begin{bmatrix} \mathbf{q} \\ \mathbf{k} \end{bmatrix} \right]. \tag{5.11}$$

Matrices $\mathbf{G}$, $\mathbf{H}$, $\mathbf{L}$, and vectors $\mathbf{p}$ and $\mathbf{a}$ depend only on geometric variables – nodal coordinates. Differentiating them with respect to coordinates of each particular node, only the elements directly related to the node of derivation are affected [10]. In that case only rows and columns that correspond to the node of derivation and its neighbours are different from zero what significantly simplifies the numerical procedure.

## 6. Examples

In order to present the situations in which, during shape optimization, geometrical mesh irregularities or boundary intersections can appear, and to verify the numerical method employed to solve the optimization problem, some examples have been studied. The interactive graphical program, called DIFOPTI [21], has been incorporated to perform the pre- and postprocessing and to present the iteration steps of the shape optimization of sections under the Saint-Venant torsion. In analysis the B.E.M. has been used.

Graphical presentation of the calculated examples (Figs. 14, 16, 18, 20, 22) contains selected pictures of the optimized section with its initial, final and some intermediate shapes appearing during the iterative optimization process. Other graphs (Figs. 15, 17, 19, 21, 23) show the evolution of objective function and restriction during the optimal design process.

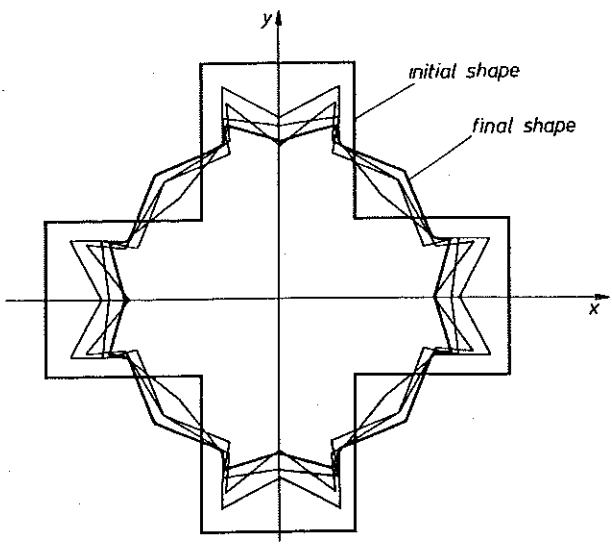


Fig. 14. Example (a). Evaluation of section's shape during the optimization process without mesh redefinition.

The first of the examples studied refers to the shape optimization of a simply-connected domain called "Greek cross" (Figs. 14, 16, 18, 20), with an obvious final result having the shape of a circle.

During the optimization process, using the graphical program DIFOPTI, a study of the influence of some geometrical irregularities on the optimization result has been made. In some examples (Figs. 14, 16) the optimization process was carried out without mesh redefinition until the final result (until the Kuhn-Tucker conditions were satisfied), while in others (Figs. 18, 20)

the mesh modification has been introduced when the geometrical irregularities appeared. In these cases, when it was necessary to eliminate nodes that caused the presence of acute angles between mesh elements, the nodes have been eliminated and then, to improve the accuracy of the optimal solution, new mesh was introduced.

For the first shape optimization of the "Greek cross", the following cases have been studied:

(a) Linear mesh elements and constant approximation of the function of unknowns without mesh redefinition (24 mesh elements, $D_0/G = 32\,\mathrm{cm}^4$, $\varepsilon_m = 10\%$, $\varepsilon_r = 3°$) (Figs. 14, 15);

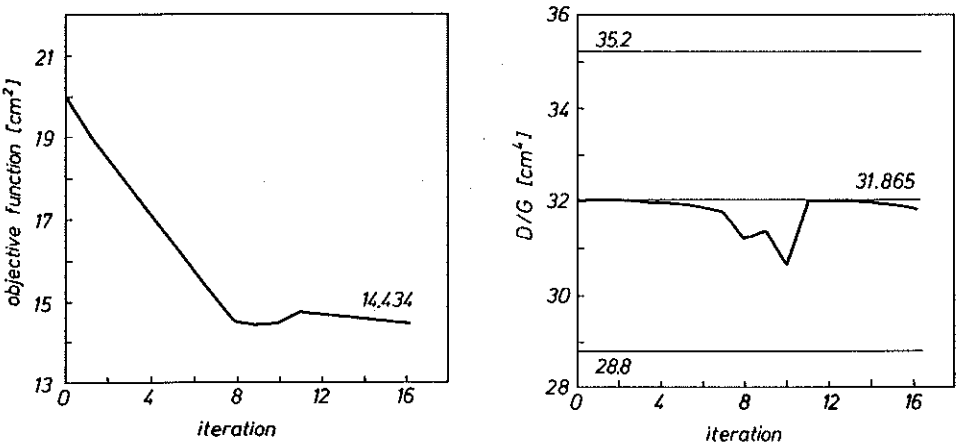


FIG. 15. Example (a). Evaluation of objective function and restriction during optimization.

(b) Linear mesh elements and linear approximation of the function of unknowns without mesh redefinition (24 mesh elements, $D_0/G = 32\,\mathrm{cm}^4$, $\varepsilon_m = 10\%$, $\varepsilon_r = 3°$) (Figs. 16, 17);

(c) Linear mesh elements and constant approximation of the function of unknowns with mesh redefinition (24 and 16 mesh elements, $D_0/G = 32\,\mathrm{cm}^4$, $\varepsilon_m = 10\%$, $\varepsilon_r = 3°$) (Figs. 18, 19);

(d) Linear mesh elements and constant approximation of the function of unknowns untill mesh redefinition and then linear approximation of the function with mesh redefinition (24 and 32 mesh elements, $D_0/G = 32\,\mathrm{cm}^4$, $\varepsilon_m = 10\%$ and $1\%$, $\varepsilon_r = 3°$ and $5°$, respectively, in both cases) (Figs. 20, 21).

It is seen in Fig. 15 that the optimization process converges rapidly with the constraint value $D_0/G$ always inside the constraint strip. However, boundary of the final design is not very smooth due to the lack of the mesh redefinition in case when geometrical mesh irregularities appear.

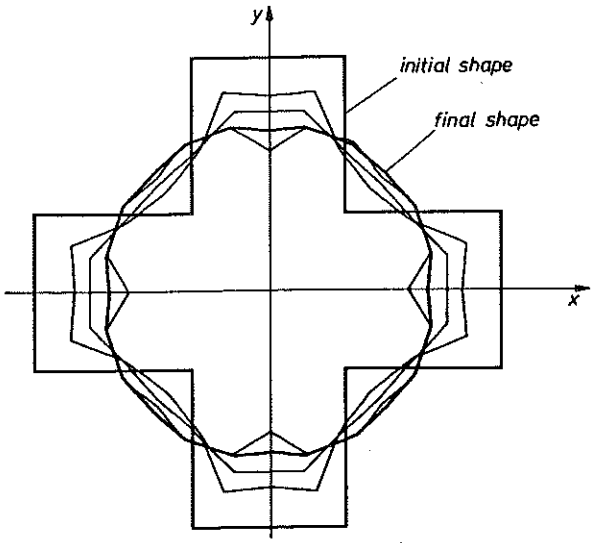


FIG. 16. Example (b). Evaluation of section's shape during the optimization process without mesh redefinition.

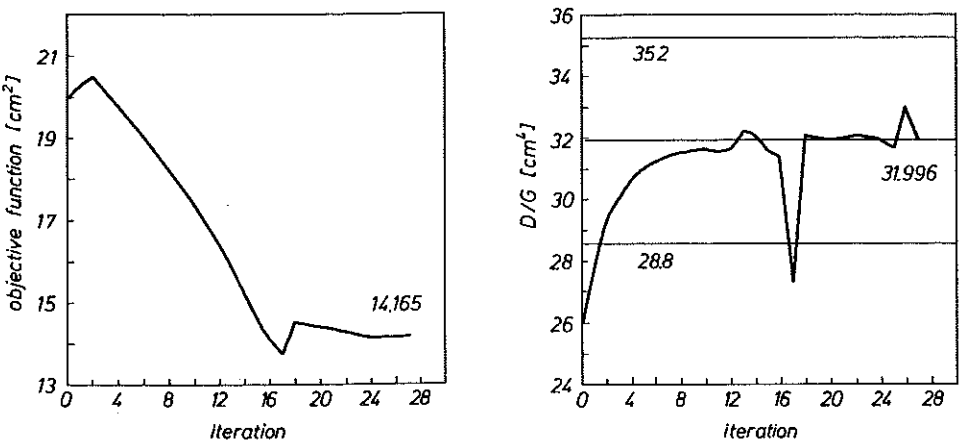


FIG. 17. Example (b). Evaluation of objective function and restriction during optimization.

In Fig. 17 it is possible to see that in Example (b) with linear approximation of unknowns, the optimization process converges to its optimal value in more steps than in Example (a), leaving in some cases the limits of restriction. The final design represents the section boundary line much more smooth than in the previous case.

In this example the mesh redefinition after the 6th iteration has been introduced. Using the DIFOPTI application, some nodes and elements have been eliminated and the boundary mesh has been modified. The sharp

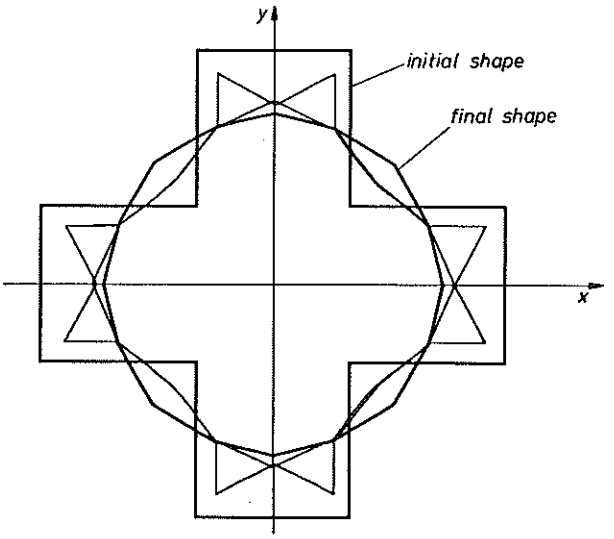


FIG. 18. Example (c). Evaluation of section's shape during the optimization process without mesh redefinition.

change in the value of objective function and restriction (Fig. 19) represents the point of mesh redefinition. The final boundary mesh, although with a lower number of elements than in Example (a), is considerably more smooth.

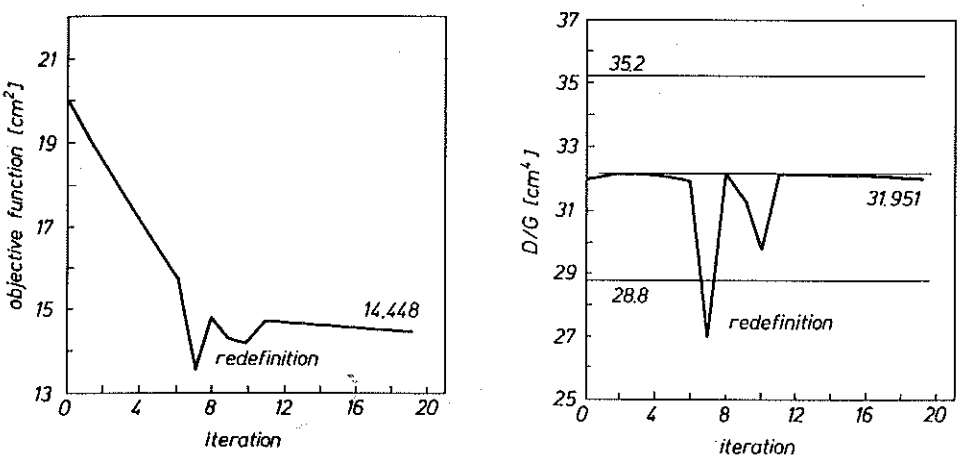


FIG. 19. Example (c). Evaluation of objective function and restriction during optimization.

In this example (Fig. 21), after elimination of the nodes and elements around the acute angles, finer boundary mesh is applied and the linear approximation of the unknowns are introduced. It was necessary to perform much more optimization steps to get the optimal solution, but it is possible

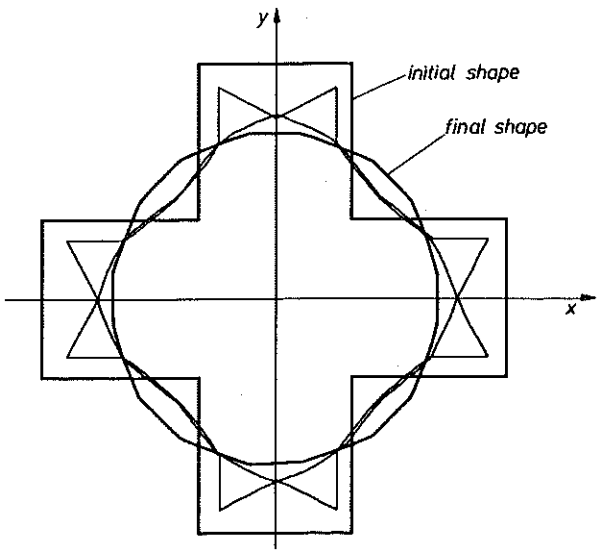


FIG. 20. Example (d). Evaluation of section's shape during the optimization process without mesh redefinition.

to stop the process almost at every step after the 25th step, without leaving the restriction strip.

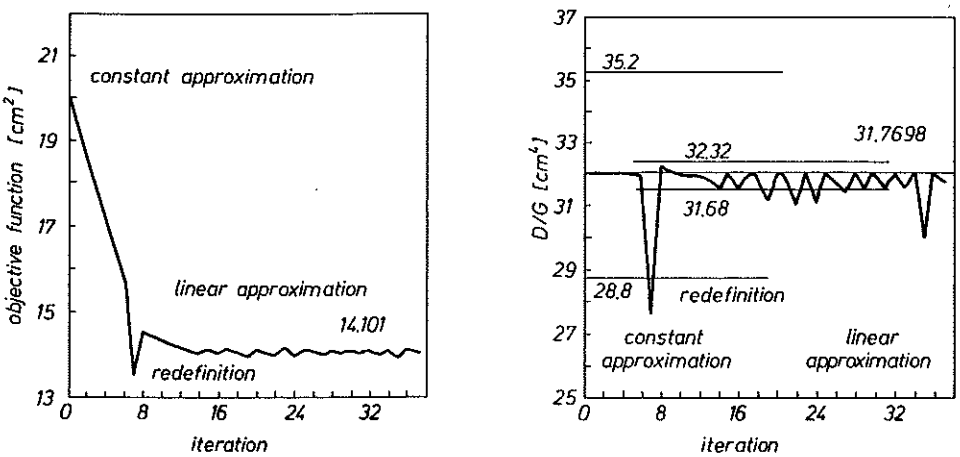


FIG. 21. Example (d). Evaluation of objective function and restriction during optimization.

The second of the studied examples concerns a triply-connected domain with an external fixed boundary and two moving holes inside. In that case the well-known solution with a single quasicircular central hole has been obtained. Here the method of boundary intersections detection has been verified. The following optimization problem has been studied:

(e) Linear mesh elements and linear approximation of the function of unknowns with mesh redefinition (72 and 80 mesh elements, $D_0/G = 1300\,\mathrm{cm}^4$, $\varepsilon_m = 2\%$ and $0.125\%$, $\varepsilon_r = 5°$ and $3°$) (Figs. 22, 23).

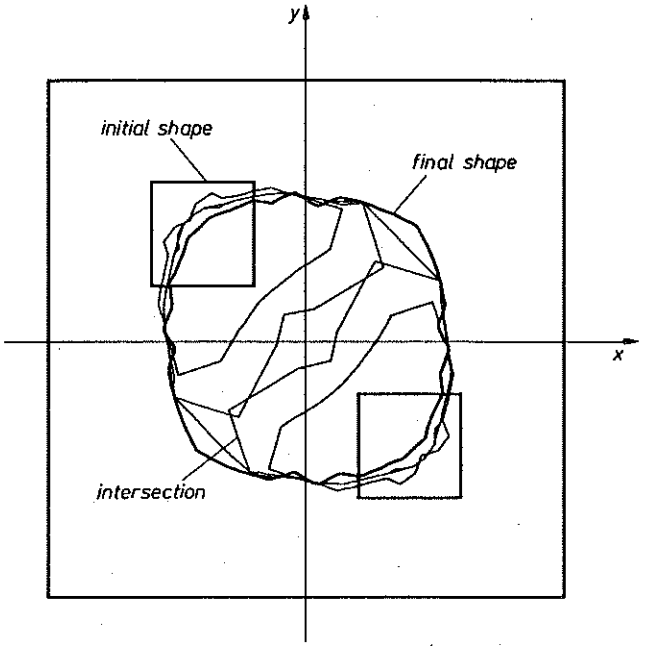


FIG. 22. Example (e). Evaluation of section's shape during the optimization process without mesh redefinition.

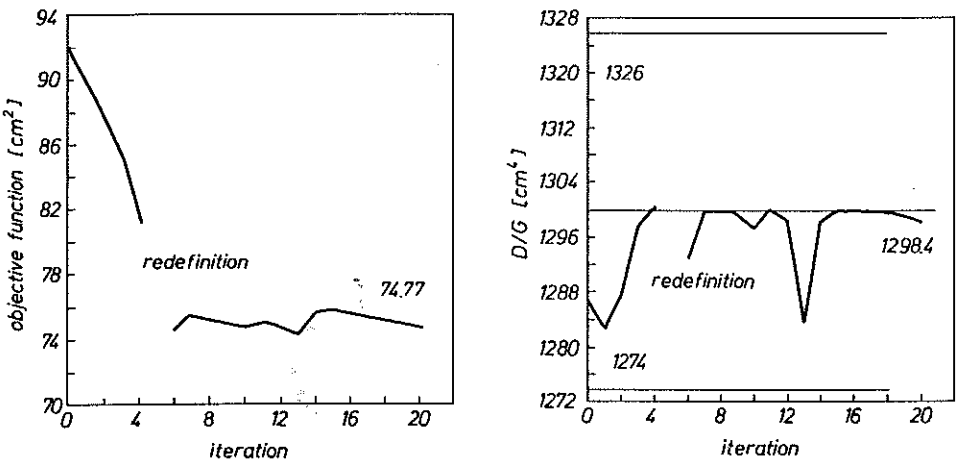


FIG. 23. Example (e). Evaluation of objective function and restriction during optimization.

In this case (Fig. 23) the intersection between internal boundaries has been detected by the program at the 5th iteration step. Using the interactive

graphical program, the intersected parts of both internal boundaries have been eliminated and one new internal boundary has been defined basing on the left nodes and elements. It has also been defined with more elements than the previous internal boundaries.

## 7. Concluding remarks

The interactive graphical program applied to the shape optimization of sections under the Saint-Venant torsion has been presented in the paper. The boundary element method has been used in the analysis, and to solve the optimization problem, a method based on the ideas of the feasible direction methods and the gradient methods have been applied.

The developed computer program enables us to modify, in an interactive way, the mesh of the optimized section at any optimization step. The necessity of mesh redefinition occurs due to existence of geometrical mesh irregularities caused by changes of coordinates of the nodes of the optimized boundary, and intersections of different boundaries in case of multiply-connected domains. It is obvious that, in some cases, disregarding the control of mesh changes can lead to erroneous results. DIFOPTI program allows us to control the optimization process and to introduce all the boundary modifications necessary to obtain the optimal design.

The authors understand that at the present stage, the DIFOPTI program has but a narrow application. However, it can easily be modified and, in the future, there exists a possibility of introduction of more adequate mesh models, automatic mesh redefinition, and other numerical methods of optimization.

## Acknowledgments

The present work has received a partial financial support from the CICYT and the IMPIVA (Spain) (research project MIT91-5015-C02-02), the Ministry of Education of Spain and Technical University of Wrocław (Poland).

## References

1. J. Sokołowski and J.-P. Zolesio, *Introduction to shape optimization*, Springer-Verlag, 1991.
2. K. Dems, *Multiparameter shape optimization of elastic bars in torsion*, Int. J. Num. Meth. in Engng., **13**, pp. 247–263, 1978.

3. N. KIKUCHI and J.E. TAYLOR, *Shape optimization of elastic bars in torsion*, Proc. of the Euromechanics Colloquium, Siegen, pp. 216–223, 1982.
4. L.M. KURSHIN and P.N. ONOPRIENKO, *Determination of the shapes of doubly connected bar sections of maximum torsional stiffness*, PMM, 40, pp. 1020–1026, 1976.
5. J.W. HOU and J.S. SHEEN, *Computational shape optimization: Recent advances and applications*, Computer Aided Optimum Design of Structures, Recent Advances, C.A. BREBBIA and S. HERNANDEZ [Eds.], Springer-Verlag, pp. 125–134, 1989.
6. C.A. MOTA, L.M. OLIVEIRA and H.C. RODRIGUES, *Optimization of the shape of solid and hollow shafts using boundary elements*, Proc. 5th Conf. on B.E.M., pp. 883–889, C.A. BREBBIA, T. FUTAGAMI and M. TANAKA [Eds.], Hiroshima 1983.
7. C.A. MOTA and K.K. CHOI, *Boundary elements in shape optimal design of structures*, Computer Aided Optimal Design, C.A. MOTA [Ed.], Vol. 2, pp. 145–185, Tróia, Portugal 1986.
8. T. BURCZYŃSKI and T. ADAMCZYK, *The boundary element method for shape design synthesis of elastic structures*, Proc. 7th Int. Conf. on B.E.M., C.A. BREBBIA and G. MAIER [Eds.], vol. 12, pp. 93–106, Springer-Verlag, 1985.
9. T. BURCZYŃSKI and T. ADAMCZYK, *The boundary element formulation for multiparameter strutures shape optimization*, Appl. Mathem. Modelling, **9**, pp. 195–200, 1985.
10. L. GRACIA, *Optimización de formas en elasticidad bidimensional mediante el método de los elementos de contorno*, PhD Thesis, University of Zaragoza, Spain 1988.
11. L. GRACIA and M. DOBLARÉ, *Shape optimization of elastic orthotropic shafts under torsion by using boundary elements*, Comp. & Struct., **30**, 6, pp. 1281–1291, 1988.
12. L. GRACIA and M. DOBLARÉ, *Shape optimization by using B.E.M.*, Proc. 10th Conf. B.E.M., C.A. BREBBIA [Ed.], Springer-Verlag, vol. 3, pp. 491–514, 1988.
13. F. ESPIGA, L. GRACIA and M. DOBLARÉ, *Shape optimization of elastic homogenous 2D bodies by the boundary element method*, Comp. & Struct., **33**, 5, pp. 1233–1241, 1989.
14. V.V. KOBELEV, *Numerical method for shape optimization using BEM*, Comp. & Struct., **33**, 5, pp. 1223–1227, 1989.
15. Z. ZHAO and R.A. ADEY, *Shape optimization using the boundary element method*, Computer Aided Optimum Design of Structures, Recent Advances, C.A. BREBBIA and S. HERNANDEZ [Eds.], Springer-Verlag, pp. 145–163, 1989.
16. Z. ZHAO and R. A. ADEY, *A numerical study on the elements of shape optimum design*, Engng. Anal. with Boundary Elem., No 9, pp. 339–349, 1992.
17. E. ATREK, *SHAPE: A Program for shape optimization of continuum structures*, Computer Aided Optimum Design of Structures, Applications, C.A. BREBBIA and S. HERNANDEZ [Eds.], Springer-Verlag, pp. 135–144, 1989.
18. S. KIBSGAARD, N. OLHOFF and J. RASMUSSEN, *Concept of an optimization system*, Computer Aided Optimum Design of Structures, Applications, C.A. BREBBIA and S. HERNANDEZ [Eds.], Springer-Verlag, pp. 79–88, 1989.
19. J.L.T. SANTOS, M.M. GODSE, K.H. CHUANG and T.A. STONE, *An iteractive system for structural design sensivity analysis and optimization*, Computer Aided Optimum Design of Structures, Applications, C.A. BREBBIA and S. HERNANDEZ [Eds.], Springer-Verlag, pp. 3–12, 1989.

20. A. ARIAS, J. CANALES and J.A. TÁRRAGO, *A parametric model of structures representation and its integration in a shape optimal design procedure*, Proc. 14th Int. Conf. on B.E.M., Springer-Verlag, C.A. BREBBIA, J. DOMÍNGUEZ and F. PARIS [Eds.], Structural Systems and Industrial Applications, pp. 401–412, 1985.

21. P. BERKOWSKI, L. GRACIA and M. DOBLARÉ, *Un programa interactivo para el diseño óptimo de formas mediante el método de los elementos de contorno*, II Congreso de Métodos Numéricos en Ingeniería, F. NAVARRINA and M. CASTELEIRO [Eds.], vol. 2, pp. 1708–1722, La Coruña 1993.

**WROCŁAW UNIVERSITY OF TECHNOLOGY,**
**INSTITUTE OF BUILDING ENGINEERING, WROCŁAW, POLAND**
**and**
**DEPARTMENTO DE INGENIERÍA CIVIL**
**C.P.S. DE LA UNIVERSIDAD DE ZARAGOZA, SPAIN.**

*Received October 26, 1994.*